Dynamics of growing surfaces by linear equations in 2+1 dimensions

Ning-Ning Pang,[1,*] Wan-Ju Li,[1] Yu-Chiao Chang,[2] Wen-Jer Tzeng,[3] and Juven Wang[1]

[1]*Department of Physics, National Taiwan University, Taipei, Taiwan, Republic of China*
[2]*Department of Mathematics, National Taiwan University, Taipei, Taiwan, Republic of China*
[3]*Department of Physics, Tamkang University, Taipei, Taiwan, Republic of China*
(Received 23 August 2006; published 17 January 2007)

An extensive study on the (2+1)-dimensional super-rough growth processes, described by a special class of linear growth equations, is undertaken. This special class of growth equations is of theoretical interests since they are exactly solvable and thus provide a window for understanding the intriguing anomalous scaling behaviors of super-rough interfaces. We first work out the exact solutions of the interfacial heights and the equal-time height difference correlation functions. Through our rigorous analysis, the detailed asymptotics of the correlation function in various time regimes are derived. Our obtained analytical results not only affirm the applicability of anomalous dynamic scaling ansatz but also offer a solid example for understanding a distinct universal feature of super-rough interfaces: the local roughness exponent is always equal to 1. Furthermore, we also perform some numerical simulations for illustration. Finally, we discuss what are the essential ingredients for constructing super-rough growth equations.

I. INTRODUCTION

Kinetic interfacial roughening phenomena have attained much interest for their generic behaviors widespread in nature's morphology [1–4]. The global interfacial widths of kinetic roughened interfaces $w(L,t)$ ($\equiv \overline{\langle [h(\mathbf{x},t) - \langle h(\mathbf{x},t) \rangle_L]^2 \rangle_L}^{1/2}$ with $h(\mathbf{x},t)$ denoting the interface height at position $\mathbf{x}$ and time t, $\langle \cdots \rangle_L$ denoting the spatial average over the whole system of lateral side length L, and the overbar denoting the statistical average), obey the following dynamic scaling ansatz:

$$w^2(L,t) = L^{2\chi} f(t/L^z), \qquad (1)$$

where $f(u) \sim u^{2\chi/z}$ for $u \ll 1$ and $f(u) \sim$ constant for $u \gg 1$. χ and z are known as the roughness exponent and the dynamic exponent, respectively. Recently, much attention has focused on super-rough growth processes, which are the growth processes with the global roughness exponent $\chi > 1$. Thus, for the super-rough interfaces, $w_{\text{sat}}(L)/L \to \infty$ as $L \to \infty$. Namely, even viewed from a very far distance, the super-rough interfaces still look rough. Their interfacial morphologies violate the usual assumption of self-affinity; i.e., the local interfacial widths bear different spatiotemporal scaling from that of global interfacial widths [5–7]. Through the extensive numerical studies, the authors in Ref. [7] proposed that the local interfacial widths $w(l,t)$ of super-rough interfaces obey the following anomalous dynamic scaling ansatz:

$$w^2(l,t) \sim \begin{cases} t^{2\chi/z} & \text{for } t^{1/z} \ll l, \\ l^{2(\chi-\kappa)} t^{2\kappa/z} & \text{for } l \ll t^{1/z} \ll L, \\ l^{2(\chi-\kappa)} L^{2\kappa} & \text{for } L \ll t^{1/z}, \end{cases} \qquad (2)$$

with l representing the side length of the local observation window.

Note that the appearance of the third nonzero exponent κ, the anomalous exponent, is the key feature of super-rough interfaces. The local roughness exponent $\chi_{\text{loc}} \equiv \chi - \kappa$ then describes the spatial scaling of the local interfacial width vs the side length of the local window. Numerous experiments have justified the above distinct features of super-rough interfaces. We list out some experiments in the following: the brain tumor growth in a petri dish [8], nickel surfaces grown by pulse-current electrodeposition [9], growth of Pt sputter deposited on glass at room temperature [10], thermal evaporation or epitaxial growth of Si films with low substrate temperature [11,12], wood fractured surfaces [13], and spontaneous imbibition of a viscous fluid in a porous medium [14]. However, relatively few analytical investigations have been done. Among these few analytical works in the literature, some pioneer works done by López *et al.* [15,16] are very enlightening. They use the renormalization-group scaling analysis to explore the general features of super-rough interfaces and obtain the following results. (1) Super-roughening may occur in conserved dynamics, but cannot take place in nonconserved growth equations. (2) The local roughness exponent $\chi_{\text{loc}} \equiv \chi - \kappa$ is always equal to 1 for the super-rough growth equations with annealed white noise. Their works are based on more conceptual frameworks and give generic concepts about super-rough interfaces. In this paper, we plan to work on a specific class of super-rough growth processes and perform detailed calculations. Our goal is to obtain more insights on interfacial super roughening through extensive studies of solid examples. We believe that these two ways of approach are equally important and complementary to each other.

In the following, we will take an extensive study on the super-rough growth phenomena described by the following class of linear growth equations in 2+1 dimensions:

$$\partial_t h(\mathbf{x},t) = (-1)^{m+1} \nu (\nabla^2)^m h(\mathbf{x},t) + \eta(\mathbf{x},t), \qquad (3)$$

with the white noise $\overline{\eta(\mathbf{x},t)\eta(\mathbf{x}',t')} = D\delta(\mathbf{x}-\mathbf{x}')\delta(t-t')$. Here, m is an arbitrary integer larger than 1. For $m=2$, Eq.

---

*Corresponding author. Electronic address: nnp@phys.ntu.edu.tw

(3) corresponds to the famous Herring-Mullins equation in $2+1$ dimensions [17]. Note that, for the Herring-Mullins equation, the global roughness exponent $\chi=1$ and thus it is right at the border between the class of super-rough interfaces ($\chi>1$) and the class of normal rough interfaces ($\chi<1$). The Herring-Mullins equation has drawn much attention since many experiments can be well described by this equation; for example, the growth of amorphous Si films by thermal evaporation with a low substrate temperature [11], the epitaxial growth of Si on Si(111) substrate [12], the sputtered etching of Si(111) surfaces [12], and Pt sputter deposited on glass at room temperature [10]. Although the experimental realizations for Eq. (3) with $m \geq 3$ have not yet been established, the study of this class of growth equations is still very valuable. It can help us to systematically understand the influence of local interfacial height correlation on the mechanism of interfacial super roughening. The outline of this paper is as follows. In Sec. II, we will first work at the explicit expression of interface configuration and numerically generate the interface morphology in a 3D plot. Then, we will analytically derive the equal-time height difference correlation function and its asymptotics in different time regimes. The implication of the obtained results will be explored, such as the comparison with equilibrium critical phenomena and formation of macroscopic structures during super-roughening processes. In Sec. III, numerical integration of Eq. (3) will be performed as numerical illustration and reconfirmation of analytical results. In Sec. IV, a conclusion will be made. We will also briefly discuss the essential ingredients of constructing super-rough growth equations and point out some possible future directions.

II. ANALYTICAL INVESTIGATION

Let us consider interface $h(\mathbf{x},t)$ defined on a two-dimensional substrate with side length L. The periodic boundary conditions and the flat initial conditions are imposed. To solve Eq. (3), use Fourier transformation

$$\widetilde{f}(\mathbf{k}_{n,l},t) \equiv \frac{1}{L^2} \int_0^L \int_0^L e^{-i\mathbf{k}_{n,l}\cdot\mathbf{x}} f(\mathbf{x},t) d\mathbf{x} \tag{4}$$

in which f denotes h or η and $\mathbf{k}_{n,l} \equiv \left(\frac{2n\pi}{L}, \frac{2l\pi}{L}\right)$ with n,l being integers. We obtain

$$\partial_t \widetilde{h}(\mathbf{k}_{n,l},t) = -\nu k_{n,l}^{2m} \widetilde{h}(\mathbf{k}_{n,l},t) + \widetilde{\eta}(\mathbf{k}_{n,l},t), \tag{5}$$

with $k_{n,l}^2 \equiv \left(\frac{2n\pi}{L}\right)^2 + \left(\frac{2l\pi}{L}\right)^2$. Under the assumption of the flat initial conditions [i.e., $h(\mathbf{x},t=0)=0$ for all $\mathbf{x}$], the solution is easily obtained

$$\widetilde{h}(\mathbf{k}_{n,l},t) = e^{-\nu k_{n,l}^{2m} t} \int_0^t e^{\nu k_{n,l}^{2m} \tau} \widetilde{\eta}(\mathbf{k}_{n,l},\tau) d\tau. \tag{6}$$

By the inverse Fourier transformation

$$f(\mathbf{x},t) = \sum_{n=-\infty}^{\infty} \sum_{l=-\infty}^{\infty} \widetilde{f}(\mathbf{k}_{n,l},t) e^{i\mathbf{k}_{n,l}\cdot\mathbf{x}}, \tag{7}$$
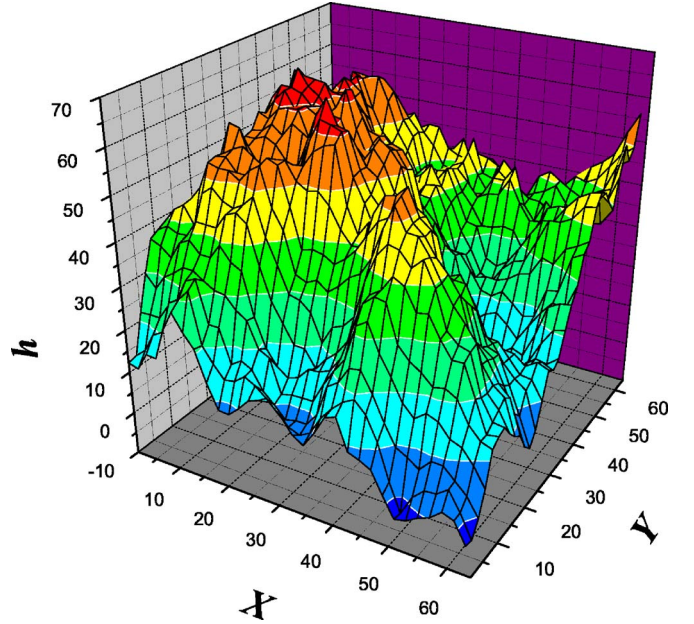
then we have

FIG. 1. (Color online) A window of the typical interfacial configuration, generated by numerical integration of Eq. (3) with $m=2$ and the rescaled parameter $r (\equiv \delta \tilde{t}/\Delta \tilde{x}^{2m}) = 0.03$. The lateral side lengths of the local window and the whole system are 64 and 256 grid points, respectively, and the simulation time t is 2^{23} time steps.

$$h(\mathbf{x},t) = \frac{1}{L^2} \int_0^t d\tau \int_{L \times L} d\boldsymbol{\xi}\, \eta(\mathbf{x}+\boldsymbol{\xi},t-\tau) \sum_{n=-\infty}^{\infty} \sum_{l=-\infty}^{\infty} e^{-i\mathbf{k}_{n,l}\cdot\boldsymbol{\xi} - \nu k_{n,l}^{2m}\tau}. \tag{8}$$

Hence, we obtain the exact expression of interface heights $h(\mathbf{x},t)$. For illustration, Fig. 1 demonstrates the typical interfacial morphology after a long growth time. From direct scaling analysis, we have the global roughness exponent $\chi = m-1$ and the dynamic exponent $z=2m$. Thus, for the growth processes described by Eq. (3) with $m \geq 3$ in $2+1$ dimensions display super-roughening phenomena. Besides, for Eq. (3) with $m=2$, it is right at the border between the super-rough regime and the normal roughness regime.

Next, we will explore the super-roughening phenomena by studying the equal-time height difference correlation functions $G(\mathbf{r},t)$, which is defined by

$$G(\mathbf{r},t) \equiv \overline{\langle (h(\mathbf{x},t) - h(\mathbf{x}+\mathbf{r},t))^2 \rangle_L}. \tag{9}$$

The calculation can be reduced by noting that

$$G(\mathbf{r},t) = \overline{\langle h^2(\mathbf{x},t)\rangle_L} + \overline{\langle h^2(\mathbf{x}+\mathbf{r},t)\rangle_L} - 2\overline{\langle h(\mathbf{x},t)h(\mathbf{x}+\mathbf{r},t)\rangle_L}. \tag{10}$$

It is straightforward to obtain, with the use of Eq. (8),

$$\overline{\langle h(\mathbf{x},t)h(\mathbf{x}+\mathbf{r},t)\rangle_L} = \frac{D}{2L^2} \sum_{n=-\infty}^{\infty} \sum_{l=-\infty}^{\infty} e^{-i\mathbf{k}_{n,l}\cdot\mathbf{r}} \frac{1-e^{-2\nu k_{n,l}^{2m} t}}{\nu k_{n,l}^{2m}}. \tag{11}$$

After some simple calculation, the equal-time height difference correlation function $G(\mathbf{r},t)$ is then obtained as follows:

$$G(\mathbf{r},t) = \frac{D}{L^2} \sum_{\substack{n=-\infty, \\ n\neq 0}}^{+\infty} \sum_{\substack{l=-\infty, \\ l\neq 0}}^{+\infty} [1 - \cos(\mathbf{k}_{n,l} \cdot \mathbf{r})] \frac{1 - e^{-2\nu k_{n,l}^{2m} t}}{\nu k_{n,l}^{2m}}.$$

$$(12)$$

It is easily seen from Eq. (12) that there exists a characteristic length in the $\mathbf{k}$-space, $k_c \equiv (2\nu t)^{-1/2m}$. It separates the time evolution of $G(\mathbf{r},t)$ into three regimes:

$$\nu t \ll r^z \Leftrightarrow \frac{1}{L} \ll \frac{1}{r} \ll k_c \quad \text{early},$$

$$r^z \ll \nu t \ll L \Leftrightarrow \frac{1}{L} \ll k_c \ll \frac{1}{r} \quad \text{intermediate},$$

$$L^z \ll \nu t \Leftrightarrow k_c \ll \frac{1}{L} \quad \text{late}. \quad (13)$$

Subsequently, we would like to study the asymptotics of $G(\mathbf{r},t)$ in these three time regimes. We will pay special attention to the intermediate and late times in which the superroughening phenomena occur. Since $k_c \gg 1/L$ in both the early and intermediate time regimes, we take the limit $L \to \infty$ and view Eq. (12) in these two regimes as a Riemann sum. Thus,

$$G(\mathbf{r},t)|_{t\ll L^z/\nu} \approx \frac{D}{4\pi^2} \int_{-\infty}^{\infty} \int_{-\infty}^{\infty} [1 - \cos(\mathbf{k} \cdot \mathbf{r})]$$

$$\times \frac{1 - e^{-2\nu k^{2m} t}}{\nu k^{2m}} dk_x dk_y. \quad (14)$$

With a simple change of variable $\mathbf{k} \equiv k_c \boldsymbol{\xi}$, Eq. (14) can then be rewritten as

$$G(\mathbf{r},t)|_{t\ll L^z/\nu} \approx \frac{D}{2\pi^2 \nu} k_c^{2-2m} \int_0^{\infty} \int_0^{\infty} [1 - \cos(k_c \boldsymbol{\xi} \cdot \mathbf{r})]$$

$$\times \frac{1 - e^{-2\xi^{2m}}}{\xi^{2m}} d\xi_x d\xi_y$$

$$= \frac{D}{2\pi^2 \nu} k_c^{2-2m} \int_0^{\infty} \int_0^{\pi/2} [1 - \cos(k_c \boldsymbol{\xi} \cdot \mathbf{r})]$$

$$\times \frac{1 - e^{-2\xi^{2m}}}{\xi^{2m-1}} d\theta d\xi$$

$$= \frac{D}{4\pi\nu} k_c^{2-2m} \int_0^{\infty} [1 - \cos(k_c \boldsymbol{\xi} \cdot \mathbf{r})] \frac{1 - e^{-2\xi^{2m}}}{\xi^{2m-1}} d\xi$$

$$\equiv \frac{D}{4\pi\nu} k_c^{2-2m} M_m. \quad (15)$$

In the early time regime $t \ll r^z/\nu$, M_m can be regarded as a constant in t. We then have

$$G(\mathbf{r},t)|_{t\ll r^z/\nu} \sim t^{2\chi/z}.$$

For the intermediate time regime, it is convenient to work in the polar coordinate. Let $\mathbf{k} = k_c \boldsymbol{\xi}$, $\boldsymbol{\xi} = (\xi \cos\theta, \xi \sin\theta)$, $\mathbf{r} = (r\cos\phi, r\sin\phi)$ and rewrite Eq. (14) as follows:

$$G(\mathbf{r},t)|_{r^z/\nu\ll t\ll L^z/\nu} \approx \frac{D}{4\pi^2\nu} k_c^{2-2m} \int_0^{\infty} \int_0^{2\pi} \{1 - \cos[k_c r\xi \cos(\theta - \phi)]\} \cdot (1 - e^{-\xi^{2m}}) \xi^{1-2m} d\theta d\xi. \quad (16)$$

We then employ the following property of Bessel functions [18]:

$$\cos(k_c r\xi \cos u) = J_0(k_c r\xi) + \sum_{j=1}^{\infty} (-1)^j J_{2j}(k_c r\xi) \cos(2ju). \quad (17)$$

By substituting Eq. (17) into Eq. (16) and integrating over θ, all the terms containing $\cos(2ju)$ vanish. Hence,

$$G(\mathbf{r},t)|_{r^z/\nu\ll t\ll L^z/\nu} \approx \frac{D}{2\pi\nu} k_c^{2-2m} \int_0^{\infty} [1 - J_0(k_c r\xi)](1 - e^{-\xi^{2m}}) \xi^{1-2m} d\xi$$

$$= \frac{D}{2\pi\nu} k_c^{2-2m} \left[\frac{m}{m-1} \int_0^{\infty} e^{-\xi^{2m}} \xi d\xi - m \sum_{p=0}^{m-2} \frac{(-1)^p \Gamma(m-p)\Gamma(m-p-1)}{\Gamma(m)\Gamma(m)} \left(\frac{k_c r}{2}\right)^{2p} \int_0^{\infty} J_0(k_c r\xi) e^{-\xi^{2m}} \xi^{1+2p} d\xi \right.$$

$$+ m \sum_{p=0}^{m-2} \frac{(-1)^p [\Gamma(m-p-1)]^2}{\Gamma(m)\Gamma(m)} \left(\frac{k_c r}{2}\right)^{2p+1} \int_0^{\infty} J_1(k_c r\xi) e^{-\xi^{2m}} \xi^{2+2p} d\xi$$

$$\left. + \frac{(-1)^m}{\Gamma(m)\Gamma(m)} \left(\frac{k_c r}{2}\right)^{2m-2} \int_0^{\infty} J_0(k_c r\xi)(1 - e^{-\xi^{2m}}) \xi^{-1} d\xi \right]. \quad (18)$$

Since $\int_0^{\infty} e^{-\xi^{2m}} \xi^p d\xi$ is finite for all $p \geq 0$, it is legitimate to substitute the power series expansion of Bessel functions [18] $J_n(x) = \left(\frac{x}{2}\right)^n \sum_{j=0}^{\infty} \frac{(-x^2/4)^j}{j!(n+j)!}$ into Eq. (18). By using the following relations for digamma functions $\psi(\cdot)$ [18],

$$\int_0^\infty x^{\alpha-1} e^{-px^\mu} \ln x \, dx = \frac{1}{\mu^2 p^{\alpha/\mu}} \Gamma(\alpha/\mu)[\psi(\alpha/\mu) - \ln p] \quad \text{with } \mu, \text{Re}(\alpha), \text{Re}(p) > 0,$$

$$\psi(1+x) = \psi(x) + \frac{1}{x} \tag{19}$$

and with some tedious calculation, we finally obtain

$$G(\mathbf{r},t)|_{r^z/\nu \ll t \ll L^z/\nu} \approx \frac{D}{4\pi\nu\Gamma(m)^2} k_c^{2-2m} \left\{ \sum_{l=1}^\infty A_l \left(\frac{k_c r}{2} \right)^{2l} + (-1)^{m-1} \left(\frac{k_c r}{2} \right)^{2m-2} \left[2\ln(k_c r) + \gamma\left(2 - \frac{1}{m} \right) \right] \right\}, \tag{20}$$

with the coefficients

$$A_l = \begin{cases} (-1)^{l-1} \Gamma\left(\dfrac{l+1}{m} \right) \sum_{p=0}^{m-2} \left[\dfrac{\Gamma(m-p-1)^2}{\Gamma(l-p+1)^2} \left(\dfrac{m-2p+l-1}{l-p} \right) \right] & \text{for } l < m, \\[3ex] (-1)^{l-1} \Gamma\left(\dfrac{l+1}{m} \right) \sum_{p=0}^{m-2} \left[\dfrac{\Gamma(m-p-1)^2}{\Gamma(l-p+1)^2} \left(\dfrac{m-2p+l-1}{l-p} \right) \right] + \dfrac{(-1)^{l-1}\Gamma\left(\dfrac{l+1}{m} \right)}{(l-m+1)[(l-m+1)!]^2} & \text{for } l \geq m \end{cases} \tag{21}$$

and $\gamma (\approx 0.577\,22)$ being Euler's constant. Recall that the global roughness exponent $\chi = m-1$ and the dynamic exponent $z=2m$. For the case with $m=2$, the most dominant term in Eq. (20) is

$$\left(\frac{-Dr^2}{8\pi\nu} \right) \ln(k_c r) = \left(\frac{Dr^2}{8\pi\nu} \right) \ln\left(\frac{(2\nu t)^{1/z}}{r} \right). \tag{22}$$

For the cases with $m \geq 3$, the most dominant term in Eq. (20) is

$$\frac{DA_1}{16\pi\nu\Gamma(m)^2} k_c^{4-2m} r^2 = \frac{DA_1}{16\pi\nu\Gamma(m)^2} r^2 (2\nu t)^{2(\chi-1)/z}. \tag{23}$$

For $m \geq 3$, the anomalous dynamic scaling behavior in the intermediate time regime is described by the leading anomalous term $t^{2(\chi-1)/z} r^2$ and the subleading anomalous terms $t^{2(\chi-2)/z} r^4, \ldots, t^{2(\chi-m+2)/z} r^{2m-4}, \ln\left(\frac{t^{1/z}}{r} \right) r^{2m-2}$ over the ordinary dynamic scaling term $r^{2\chi}$. We conclude that

$$G(\mathbf{r},t) \sim r^{2(\chi-\kappa)} t^{2\kappa/z} \quad \text{for } r \ll t^{1/z} \ll L \quad \text{and} \quad m \geq 3. \tag{24}$$

Thus, the anomalous exponent $\kappa = \chi - 1$ and the local roughness exponent $\chi_{\text{loc}} = 1$. Note that for the case with $m=2$, the anomalous exponent $\kappa = 0$ and we have $G(\mathbf{r},t) \sim r^{2\chi} \ln\left(\frac{t^{1/z}}{r} \right)$. Here, we have rigorously derived the logarithmic correction on the equal-time height difference correlation function, when the exponent κ is equal to zero. This logarithmic correction on the relevant quantities, when the corresponding scaling exponent is equal to zero, has been widely observed in many equilibrium critical phenomena. For example, in two-dimensional Ising model, the specific heat exponent $\alpha = 0$ and the specific heat C_v is then proportional to $\ln\left(\frac{|T-T_c|}{T_c} \right)$ [19]; in site percolation problems with $p < p_c$, the mass of the largest cluster $M(L) \sim \ln L$ with L being the side length of the system [20]; in the scattered radiation through fluids at frequencies on the order of ω_B (the Brillouin doublet) ≈ 1 MHz, the sound velocity $v_s \sim |\ln\left(\frac{|T-T_c|}{T_c} \right)|^{-1/2}$ [19]. To our knowledge, our result is the first analytical derivation which rigorously shows this logarithmic correction also occurring in the dynamic interfacial-roughening process, a process far from equilibrium.

Subsequently, for the late time regime $t \gg L^z/\nu$, we now have $k_c \ll 1/L$ and

$$G(\mathbf{r},t)|_{t \gg L^z/\nu} \approx \frac{D}{\nu} \int_{r_0}^\infty \int_0^{2\pi} [1 - \cos(\mathbf{k}\cdot\mathbf{r})] \frac{1-e^{-2\nu t k^{2m}}}{k^{2m-1}} d\theta \, dk$$

$$= \frac{2\pi D}{\nu} \int_{r_0}^\infty [1-J_0(kr)](1-e^{-2\nu t k^{2m}}) k^{1-2m} dk, \tag{25}$$

with $\pi r_0^2 \equiv \left(\frac{2\pi}{L} \right)^2$. To make the calculation simpler by letting $k \equiv r_0 \xi$ and $\alpha \equiv 2\nu t r_0^{2m}$, Eq. (25) can be recast as

$$G(\mathbf{r},t)|_{t \gg L^z/\nu} = \frac{2\pi D}{\nu} r_0^{2-2m} \int_1^\infty [1 - J_0(r_0 r \xi)]$$

$$\times (1 - e^{-\alpha\xi^{2m}}) \xi^{1-2m} d\xi. \tag{26}$$

The late time regime $t \gg L^z/\nu$ implies that it is legitimate to take the limit $\alpha \to \infty$. By using the properties of Bessel functions and digamma functions [18] and with some tedious calculations, we finally derive

$$G(\mathbf{r},t)|_{t \gg L^z/\nu} = \frac{2\pi D}{\nu} r_0^{2-2m} \left\{ (-1)^{m+1} \frac{1}{\Gamma(m)^2} \left(\frac{r_0 r}{2} \right)^{2m-2} \right.$$

$$\left. \times \left[\ln\left(\frac{r_0 r}{2} \right) + \gamma \right] + \sum_{l=1}^\infty B_l \left(\frac{r_0 r}{2} \right)^{2l} \right\}, \tag{27}$$

with the coefficients

$$B_l = \begin{cases} \dfrac{(-1)^l}{\Gamma(m)^2} \sum\limits_{p=1}^{m-1} \dfrac{(2l-2p+1)\Gamma(m-p)^2}{(2l-2p+2)\Gamma(l-p+1)^2} + \dfrac{(-1)^l}{(2-2m)\Gamma(l+1)^2} & \text{for } l < m, \\[3ex] \dfrac{(-1)^l}{\Gamma(m)^2} \sum\limits_{p=1}^{m-1} \dfrac{(2l-2p+1)\Gamma(m-p)^2}{(2l-2p+2)\Gamma(l-p+1)^2} + \dfrac{(-1)^l}{(2-2m)\Gamma(l+1)^2} + \dfrac{(-1)^l}{4\Gamma(m)^2(l-m+1)[(l-m+1)!]^2} & \text{for } l \ge m \end{cases} \tag{28}$$

and γ being Euler's constant. For the case with $m=2$, the most dominant term in Eq. (27) is

$$-\frac{\pi D}{2\nu\Gamma(m)^2} r^2 \ln(r_0 r) \approx \frac{\pi D}{2\nu\Gamma(m)^2} r^2 \ln(L/r). \tag{29}$$

For the cases with $m \ge 3$, the most dominant term in Eq. (27) is

$$\frac{\pi D B_1}{2\nu} r_0^{4-2m} r^2 = \frac{\pi D B_1}{2\nu} (4\pi)^{2-m} r^2 L^{2(\chi-1)}. \tag{30}$$

For $m \ge 3$, the anomalous dynamic scaling behavior in the late time regime is described by the leading anomalous term $L^{2(\chi-1)}r^2$ and the subleading anomalous terms $L^{2(\chi-2)}r^4, \ldots, L^{2(\chi-m+2)}r^{2m-4}, \ln(L/r)r^{2m-2}$ over the ordinary dynamic scaling term $r^{2\chi}$.

Besides, for the growth process described by Eq. (3) with $m=2$ in $2+1$ dimensions, we have the global roughness exponent $\chi=1$ and the logarithmic corrections in the asymptotics of $G(\mathbf{r},t)$ appear in the intermediate and late time regimes. Note that the range of the spatial correlation between the interfacial heights has reached the lateral side length L of the substrate in the late time regime. Thus, $G(\mathbf{r},t)$ no more increases with time at this stage. With some observation, we see that the asymptotics of $G(\mathbf{r},t)$ in the intermediate and late time regimes have very similar forms in structure. By replacing t in the intermediate time asymptotics with $O(L^z/\nu)$, one obtains the asymptotics of $G(\mathbf{r},t)$ in the late time regime. Namely, the lateral side length L of the substrate enters as an important cutoff. For an infinite system size $(L \to \infty)$, $G(\mathbf{r},t)$ can always increase with time and go to infinity. This is exactly the manifestation of local interfacial orientational instability.

To understand the geometrical reasons behind the appearance of anomalous dynamic scaling behaviors of the correlation function, we then generate interface configurations in 3D plots. We observe that the interface morphology gradually develops large and irregular mounds as the growth time increases. These observed mounds differ from those in the Schwoebel barrier models in which the large-scale pyramids of uniform size are formed [2,3]. For illustration, Fig. 1 shows the typical interfacial configuration after a long growth time for Eq. (3) with $m=2$ in $2+1$ dimensions. As the value of m increases, the mounds appear even larger and rougher due to less restriction on the local interfacial slope variation. The formation of macroscopic structures is the key reason for the appearance of anomalous dynamic scaling behaviors. Leschhorn and Tang in Ref. [21], by applying the Schwartz inequality, have shown that the local roughness

exponent $\chi_{loc} \le 1$ for any interfacial roughening processes (including both normal roughening and super roughening). On the other hand, López *et al.* [15,16] use the dynamic renormalization group analysis and obtain the local roughness exponent $\chi_{loc}=1$ for the super-rough growth equations with annealed white noise. Here, we plan to give the reasoning about $\chi_{loc}=1$ for super-roughening processes, from geometric point of view. As we have mentioned and illustrated in Fig. 1, the super-rough growth processes are associated with the formation of macroscopic structures. It is the formation of macroscopic structures which results in the following scaling terms $\sum_{q=1}^{\infty} A_{2q} t^{2(\chi-q)/z} r^{2q}$ in the intermediate time regime $r^z/\nu \ll t \ll L^z/\nu$ and $\sum_{q=1}^{\infty} B_{2q} L^{2(\chi-q)} r^{2q}$ in the late time regime $L^z/\nu \ll t$. It is clear that, for the global roughness exponent $\chi > 1$, the most leading anomalous term is $t^{2(\chi-1)/z} r^2$ in the intermediate time regime and $L^{2(\chi-1)} r^2$ in the late time regime, which dominate over the stochastic-induced ordinary scaling term $r^{2\chi}$. Compared with the anomalous dynamic scaling ansatz, we then have $\chi_{loc}=1$ and the anomalous scaling exponent $\kappa \equiv \chi - \chi_{loc} = \chi - 1$. If we view these anomalous scaling terms in $G(\mathbf{r},t)$ as the power series expansion of the contribution due to macroscopic structure formation, the above argument can also be applied to explain $\chi_{loc}=1$ for interfacial super roughening with correlated noise or quenched noise [22].

Finally, it is well known that the square of local interfacial width $w^2(l,t)$ bears the same scaling behaviors as those of the equal-time height difference correlation function $G(\mathbf{r},t)$; i.e., by simply replacing r in the asymptotics of $G(\mathbf{r},t)$ with $O(l)$, one immediately obtains the asymptotics of $w^2(l,t)$. For illustration and numerical reconfirmation, we will numerically generate the local interfacial widths in the next section.

III. NUMERICAL ILLUSTRATION

In the following, we will perform numerical integration of Eq. (3) in $2+1$ dimensions with $m=2$ and 3 as illustrative examples. We first derive the discretized form of Eq. (3) as follows:

$$\frac{\bar{h}(\mathbf{x}_j, t_{n+1}) - \bar{h}(\mathbf{x}_j, t_n)}{\delta t} = (-1)^{m+1} \nu \left(\sum_{i=1}^{d} \frac{S_{\mathbf{e}_i} - 2\mathbb{I} + S_{-\mathbf{e}_i}}{\Delta x^2} \right)^m \bar{h}(\mathbf{x}_j, t_n)$$
$$+ \bar{\eta}(\mathbf{x}_j, t_n), \tag{31}$$

where $\bar{h}(\mathbf{x}_j, t_n)$ denotes the average of $h(\mathbf{x},t)$ over a d-dimensional cube of side length Δx, centered at the position $\mathbf{x}_j$, and over the time interval δt, centered at time t_n. Here, $\mathbb{I}$ denotes the identity operator and $S_{\mathbf{e}_i}$ denotes a shift-

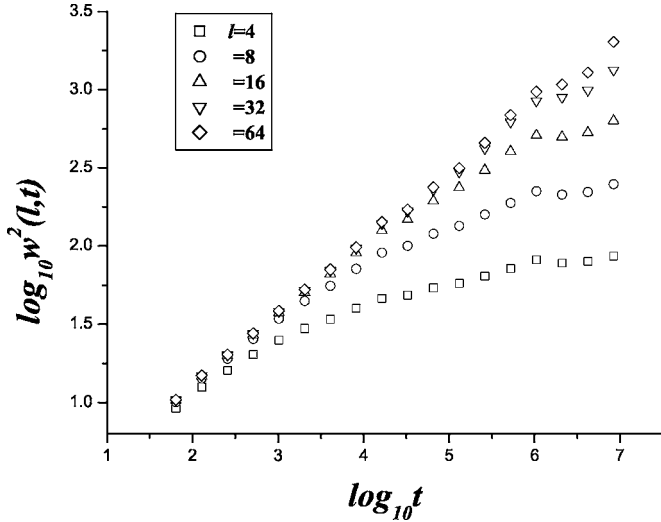FIG. 2. The log-log plot of $w^2(l,t)$ vs time t for Eq. (3) with $m=2$ in $2+1$ dimensions. The side lengths of the local windows are $l=4, 8, 16, 32,$ and 64 grid points. The rescaled parameter in Eq. (33), $r \equiv \delta \tilde{t}/\Delta \tilde{x}^{2m}$, is set to be 0.001.

ing operator; i.e., $S_{\mathbf{e}_i} f(\mathbf{x}_j, t_n) = f(\mathbf{x}_j + \mathbf{e}_i, t_n)$ with $\mathbf{e}_i$ representing the position unit vector along the ith axis. $\overline{\eta}(\mathbf{x}_j, t_n)$ denotes the average of $\eta(\mathbf{x}, t)$ over the very same cube and the time interval. The correlation for $\overline{\eta}(\mathbf{x}_j, t_n)$ is

$$\langle \overline{\eta}(\mathbf{x}_{j'}, t_{n'}) \overline{\eta}(\mathbf{x}_j, t_n) \rangle = \frac{D}{\Delta x^d \delta t} \left(\prod_{i=1}^{d} \delta_{j_i, j_i'} \right) \delta_{n, n'}. \quad (32)$$

By rescaling $\tilde{t}/t = \nu$, $\tilde{x}/x = 1$, and $\tilde{h}/\overline{h} = \sqrt{\nu \Delta \tilde{x}^d/(D \delta \tilde{t})}$, we have

$$\tilde{h}(\tilde{\mathbf{x}}_j, \tilde{t}_{n+1}) - \tilde{h}(\tilde{\mathbf{x}}_j, \tilde{t}_n) = (-1)^{m+1} \frac{\delta \tilde{t}}{\Delta \tilde{x}^{2m}} \left[\sum_{i=1}^{d} (S_{\tilde{\mathbf{e}}_i} - 2\mathbb{I} + S_{-\tilde{\mathbf{e}}_i}) \right]^m$$

$$\times \tilde{h}(\tilde{\mathbf{x}}_j, \tilde{t}_n) + \tilde{\eta}(\tilde{\mathbf{x}}_j, \tilde{t}_n), \quad (33)$$

with $\langle \tilde{\eta}(\mathbf{x}_{j'}, t_{n'}) \tilde{\eta}(\mathbf{x}_j, t_n) \rangle = (\prod_{i=1}^{d} \delta_{j_i, j_i'}) \delta_{n, n'}$. There remains only one adjustable parameter $r \equiv \frac{\delta \tilde{t}}{\Delta \tilde{x}^{2m}}$. As the value of r decreases, the computation accuracy is enhanced.

In numerical integration, the lateral system size is chosen to be $L \times L = 256 \times 256$ grid points. The periodic boundary conditions are imposed. The initial configuration is chosen to be flat. First, for Eq. (3) with $m=2$, the theoretical value of the global roughness exponent $\chi = 1$. Thus this case is right at the border between the class of super-rough interfaces ($\chi > 1$) and the class of normal rough interfaces ($\chi < 1$). Figure 2 shows the log-log plot of the square of local interfacial width $w^2(l,t)$ vs time t for Eq. (3) with $m=2$ in $2+1$ dimensions. The side lengths of the local windows are 4,8,16,32, and 64 grid points. The rescaled parameter in Eq. (33), $r = \frac{\delta \tilde{t}}{\Delta \tilde{x}^{2m}}$, is set to be 0.001. Figure 3 then gives excellent data collapse of $w^2(l,t)/l^{2\chi}$ vs t/l^z in a log-log plot. The theoretical values of the exponents, obtained in Sec. II, are $\chi = 1$ and $z = 4$. Through the analysis of numerical data, we find that the dynamic exponent $z = 4$ is a very strong condition in order to obtain good data collapse in Fig. 3. In the early time regime,
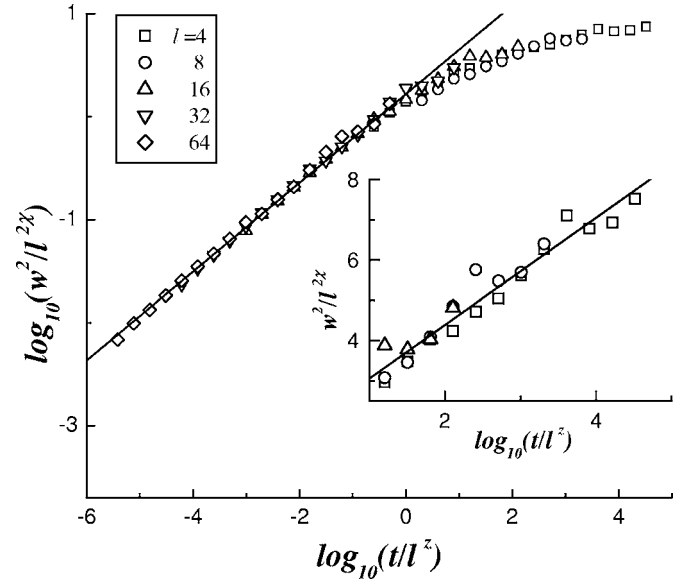

FIG. 3. The data collapse of $w^2(l,t)/l^{2\chi}$ vs t/l^z in a log-log plot for Eq. (3) with $m=2$ in $2+1$ dimensions. The side lengths of the local windows are $l=4,8,16,32,$ and 64 grid points. The values of the exponents are $\chi = 0.862 \pm 0.006$ and $z = 4$. The inset shows $w^2 \sim l^{2\chi} \log_{10}(t/l^z)$ in the intermediate time regime $l^z \ll t \ll L^z$.

$t \ll l^z$, the straight line in Fig. 3 is obtained through the least-squares-fit and the slope is 0.431 ± 0.003, which in turn gives the numerical value of the global roughness exponent $\chi = 0.862 \pm 0.006$. The discrepancy between the theoretical value and the numerical value is due to the finite size effect. However, in $2+1$ dimensions, the computation is very CPU-time consuming. The limitation of the relatively small system size is unavoidable. Recall that, in Sec. II, we analytically obtain the logarithmic temporal dependence of the local interfacial width in the intermediate time regime, $l^z \ll t \ll L^z$, for the case with $m=2$. The inset of Fig. 3 shows a nice confirmation of analytical prediction.

Next, we proceed to perform numerical integration of Eq. (3) with $m=3$. Figure 4 shows the log-log plot of the square of local interfacial width $w^2(l,t)$ vs time t, with the side lengths of the local windows $l=4,8,16,$ and 32 grid points. The rescaled parameter in Eq. (33) is set to be $r=0.003$. In Fig. 5, we obtain nice data collapse of $w^2(l,t)/l^{2\chi}$ vs t/l^z in a log-log plot. The theoretical values of the exponents, obtained in Sec. II, are $\chi = 2$, $z = 6$, and $\kappa = 1$. The straight lines in Fig. 5 are obtained through the least-squares-fit and the slopes are 0.587 ± 0.002 in the early time regime $t \ll l^z$ and 0.315 ± 0.008 in the intermediate time regime $l^z \ll t \ll L^z$. Again, the dynamic exponent $z = 6$ is a very strong condition for obtaining nice data collapse in Fig. 5. The values of the slopes in Fig. 5 in turn give the numerical values of the exponents $\chi = 1.761 \pm 0.006$ and $\kappa = 0.95 \pm 0.03$. The discrepancy between the numerical values and the theoretical values is due to the finite size effect.

IV. CONCLUSION

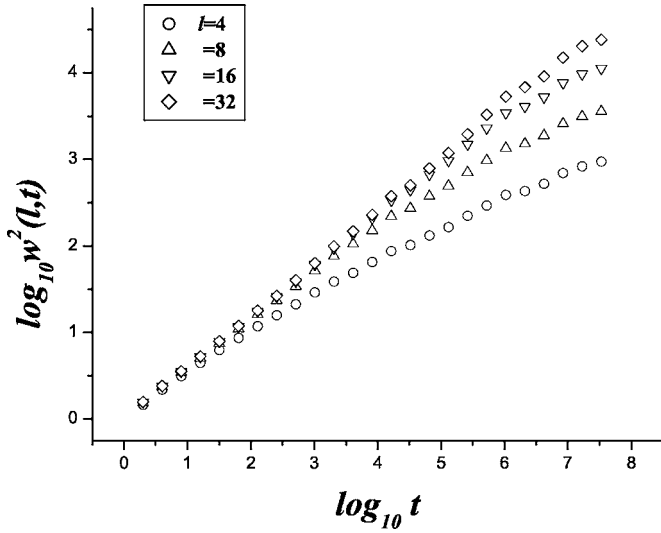In conclusion, interfacial super-roughening phenomena have attracted much interest, for their interfacial morpholo-

FIG. 4. The log-log plot of $w^2(l,t)$ vs time t for Eq. (3) with $m=3$ in 2+1 dimensions. The side lengths of the local windows are $l=4,8,16$, and 32 grid points. The rescaled parameter in Eq. (33), $r \equiv \frac{\delta t}{\Delta \tilde{x}^{2m}}$, is set to be 0.003.

gies violating the usual assumption of self-affinity. We take an extensive study on a class of super-rough interfacial growth processes in 2+1 dimensions with finite side length L of the substrate. This class of super-rough growth processes is described by linear growth equations, Eq. (3). These equations are linear and thus exactly solvable, which open a window for understanding the intriguing anomalous properties of super-rough interfaces. In this paper, we have worked out the explicit expressions of the interface heights and the correlation functions. The detailed asymptotics of the correlation functions and the local interfacial widths in all the time regimes are also analytically derived and numerically justified. We also have explicitly obtained all the dominant
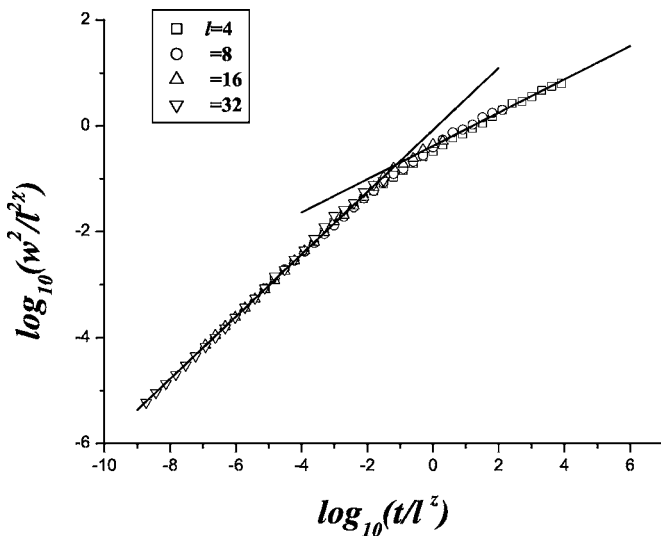

FIG. 5. The data collapse of $w^2(l,t)/l^{2\chi}$ vs t/l^z in a log-log plot for Eq. (3) with $m=3$ in 2+1 dimensions. The side lengths of the local windows are $l=4,8,16$, and 32 grid points. The values of the exponents are $\chi=1.761\pm0.006$, $\kappa=0.95\pm0.03$, and $z=6$.

anomalous scaling terms over the ordinary dynamic scaling term $r^{2\chi}$ of the correlation function. Namely, for the cases with $m\geq3$, the anomalous dynamic scaling behavior in the intermediate time regime is described by the leading anomalous term $t^{2(\chi-1)/z}r^2$ and the sub-leading anomalous terms $t^{2(\chi-2)/z}r^4,\dots,t^{2(\chi-m+2)/z}r^{2m-4},\ln\left(\frac{t^{1/z}}{r}\right)r^{2m-2}$ over the ordinary dynamic scaling term $r^{2\chi}$; in the late time regime, the anomalous dynamic scaling behavior is described by the leading anomalous term $L^{2(\chi-1)}r^2$ and the subleading anomalous terms $L^{2(\chi-2)}r^4,\dots,L^{2(\chi-m+2)}r^{2m-4},\ln(L/r)r^{2m-2}$ over the ordinary dynamic scaling term $r^{2\chi}$.

In Ref. [23], López *et al.* studied the structure factors $S(k,t)\equiv\widetilde{h}(k,t)\widetilde{h}(-k,t)$ of the 1+1 dimensional interfaces. They conjectured that the structure factors of all the 1+1 dimensional super-rough interfaces obey the ordinary dynamic scaling ansatz: $S(k,t)=k^{-(2\chi+1)}f(kt^{1/z})$, with $f(u)\sim u^{2\chi+1}$ for $u\ll1$ and $f(u)\sim$ constant for $u\gg1$. By employing the scaling analysis, they showed that for the interfaces with the global roughness exponent $\chi>1$, the equal-time height difference correlation functions (obtained from the integration of the structure factors obeying the ordinary scaling form) will obey the anomalous dynamic scaling ansatz with the local roughness exponent $\chi_{loc}=1$. Note that their analysis is based on the assumption about the scaling form of the structure factors. They then numerically studied Eq. (3) with $m=2$ in 1+1 dimensions and used this example to justify the above assumption. Their work is based on more conceptual frameworks. In this paper, we choose to work on a specific class of super-rough growth processes and perform rigorous calculations. From direct scaling analysis, we have the global roughness exponent $\chi=(2m-d)/2$ and the dynamic exponent $z=2m$, for the growth processes described by Eq. (3) in $d+1$ dimensions. From Eq. (6), we easily derive the corresponding structure factors in $d+1$ dimensions as follows:

$$S(\mathbf{k},t)=[1-\exp(-2\nu k^{2m}t)]/(\nu k^{2m})=k^{-(2\chi+d)}g(kt^{1/z}),$$

$$(34)$$

with $g(u)\sim u^{2\chi+d}$ for $u\ll1$ and $g(u)\sim$ constant for $u\gg1$. So, we conclude that for the growth processes described by Eq. (3) in $d+1$ dimensions, the structure factors obey the ordinary dynamic scaling ansatz, verifying the conjecture given in Ref. [23]. However, it is not clear whether this assumption in Ref. [23] (about the scaling form of the structure factors of super-rough interfaces) is generally true.

Note that, for $m=2$, Eq. (3) corresponds to the famous Herring-Mullins equation, which is a plausible description of various deposition experiments in industry. Besides the applications in industry, the Herring-Mullins equation in 2+1 dimensions is of theoretical interest by its own, since it is right at the border between the class of super-rough interfaces ($\chi>1$) and the class of normal rough interfaces ($\chi<1$). The Herring-Mullins equation in 2+1 dimensions has the global roughness exponent $\chi=1$, the local roughness exponent $\chi_{loc}=1$, and thus the anomalous exponent $\kappa=0$. In this paper, we rigorously obtain the logarithmic correction on the equal-time height difference correlation function and the local interfacial width, when the anomalous exponent κ is equal to zero. This logarithmic correction on the relevant

quantities, when the corresponding scaling exponent is equal to zero, has been widely observed in many equilibrium critical phenomena, such as two-dimensional Ising model, site percolation problems, and scattered radiation through fluids, etc. Our result is the first analytical derivation which rigorously shows this logarithmic correction also occurring in the dynamic interfacial roughening process, a process far from equilibrium.

Although the experimental realizations for Eq. (3) with $m \geq 3$ have not yet been established, the study of this class of growth equations is still very valuable. It can help us to capture a deeper insight about the influence of local interfacial height correlation on the mechanism of interfacial super roughening. Through numerically generating the interface morphology governed by Eq. (3) with $m \geq 2$, we observe that the interface configuration gradually develops large and irregular mounds as the growth time increases. Namely, the interfaces develop macroscopic structures. As the value of m increases, the mounds appear even larger and rougher due to less restriction on the local interfacial slope variation. Specifically, for Eq. (3) with $m \geq 2$ in $2+1$ dimensions, we obtain the global roughness exponent $\chi = m-1$, the dynamic exponent $z = 2m$, the local roughness exponent $\chi_{loc} = 1$, and the anomalous exponent $\kappa = m-2$. From geometric point of view, it is the formation of macroscopic structures which results in the following scaling terms in $G(\mathbf{r}, t)$: $\sum_{q=1}^{\infty} A_{2q} t^{2(\chi-q)/z} r^{2q}$ in the intermediate time regime $r^z/\nu \ll t \ll L^z/\nu$ and $\sum_{q=1}^{\infty} B_{2q} L^{2(\chi-q)} r^{2q}$ in the late time regime $L^z/\nu \ll t$. For the cases with the global roughness exponent $\chi > 1$, the most leading anomalous term is $t^{2(\chi-1)/z} r^2$ in the intermediate time regime and $L^{2(\chi-1)} r^2$ in the late time regime, which dominate over the stochastic-induced ordinary scaling term $r^{2\chi}$. Thus, we have the local roughness exponent χ_{loc} always equal to 1, independent of the value of m.

All the super-rough growth processes are associated with local interfacial orientational instability. However, for a real physical system with the restriction of finite system size, the local interfacial tilt cannot go to infinity. Consequently, the interfacial configurations form large mounds or grooves. So people may wonder what are the essential ingredients for constructing super-rough growth equations. Qualitatively, the interfacial kinetic roughening process can be viewed as the interplay of two effects: the smoothing effect due to local interface height correlation and the roughening effect due to noise. Thus, for a system susceptible to strong roughening effect but consisting of only weak smoothing mechanism, this system then will generate super-rough interfaces. Specifically, as the order of the derivative of h (interface height) in the interface growth equation increases or the substrate dimensionality decreases, the smoothing effect is lowered. Besides, as the shot noise correlation increases from the short-range correlation to the long-range positive correlation, the roughening effect is greatly enhanced. In this paper, we mainly focus on the influence of the order of the derivative of h on interfacial super-roughening phenomena. In our future work, we plan to extensively investigate the role of noise on interfacial super-roughening phenomena and its link to fractional Brownian motion [20].

ACKNOWLEDGMENTS

[1] T. Halpin-Healy and Y.-C. Zhang, Phys. Rep. **254**, 215 (1995).

[2] A. Pimpinelli and J. Villain, *Physics of Crystal Growth* (Cambridge University Press, Cambridge, UK, 1998).

[3] A. L. Barabási and H. E. Stanley, *Fractal Concepts in Surface Growth* (Cambridge University Press, New York, 1995).

[4] J. Krug, Adv. Phys. **46**, 139 (1997).

[5] M. Schroeder, M. Siegert, D. E. Wolf, J. D. Shore, and M. Plischke, Europhys. Lett. **24**, 563 (1993).

[6] M. Kotrla and P. Šmilauer, Phys. Rev. B **53**, 13777 (1996).

[7] S. Das Sarma, C. J. Lanczycki, R. Kotlyar, and S. V. Ghaisas, Phys. Rev. E **53**, 359 (1996).

[8] A. Brú, J. M. Pastor, I. Fernaud, I. Brú, S. Melle, and C. Berenguer, Phys. Rev. Lett. **81**, 4008 (1998).

[9] M. Saitou, Phys. Rev. B **66**, 073416 (2002).

[10] J. H. Jeffries, J. K. Zuo, and M. M. Craig, Phys. Rev. Lett. **76**, 4931 (1996).

[11] H.-N. Yang, Y.-P. Zhao, G.-C. Wang, and T.-M. Lu, Phys. Rev. Lett. **76**, 3774 (1996).

[12] H.-N. Yang, G.-C. Wang, and T.-M. Lu, Phys. Rev. Lett. **73**, 2348 (1994); Phys. Rev. B **50**, 7635 (1994).

[13] S. Morel, J. Schmittbuhl, J. M. López, and G. Valentin, Phys. Rev. E **58**, 6999 (1998).

[14] J. Soriano, A. Mercier, R. Planet, A. Hernández-Machado, M. A. Rodríguez, and J. Ortín, Phys. Rev. Lett. **95**, 104501 (2005).

[15] J. M. López, Phys. Rev. Lett. **83**, 4594 (1999).

[16] J. M. López, M. Castro, and R. Gallego, Phys. Rev. Lett. **94**, 166103 (2005).

[17] W. W. Mullins, J. Appl. Phys. **28**, 333 (1957).

[18] See, for example, *An Atlas of Functions*, edited by J. Spanier and K. B. Oldham (Springer-Verlag, Berlin, 1987); *Integrals and Series*, edited by A. P. Prudnikov, Y. A. Brychkov, and O. I. Marichev (Gordon and Breach, New York, 1986).

[19] H. E. Stanley, *Introduction to Phase Transitions and Critical Phenomena* (Oxford University Press, New York, 1971).

[20] J. Feder, *Fractals* (Plenum, New York, 1988).

[21] H. Leschhorn and L.-H. Tang, Phys. Rev. Lett. **70**, 2973 (1993).

[22] N.-N. Pang and W.-J. Tzeng, Phys. Rev. E **59**, 234 (1999).

[23] J. M. López, M. A. Rodríguez, and R. Cuerno, Physica A **246**, 329 (1997).